Compressible Separated Flows

H. L. Petrie*
Pennsylvania State University, State College, Pennsylvania
M. Samimy†
The Ohio State University, Columbus, Ohio
and
A. L. Addy‡
University of Illinois at Urbana-Champaign, Urbana, Illinois

An experimental investigation of compressible, two-dimensional, planar turbulent flows with large separated regions is presented. Three backward-facing step-flow configurations were investigated to gain a detailed knowledge of the mean flow and turbulent field in developing compressible turbulent free shear layers and the adjacent recirculating flow. Two-channel coincident laser Doppler velocimeter measurements, surface static pressure measurements, Schlieren flow visualization, and surface oil flow visualization were used to study these flows. The recirculating flows stimulated increased mixing layer growth and entrainment rates. The turbulent field of the compressible mixing layer was considerably more anisotropic than the incompressible counterpart with a decrease in the transverse velocity component turbulence intensity and the Reynolds shear stress. Laser Doppler velocity bias effects and bias corrections are demonstrated and discussed.

Introduction

THE near wake base region of blunt-based missile-type bodies at supersonic freestream Mach numbers presents challenges to experimentalists, analytical modelers, and computationalists alike. These base flows contain a large separated region bounded by the freestream and propulsive jet flow free shear layers. The bounding shear layers merge and change direction in a highly turbulent recompression zone. Although base flow modeling methods like the Chapman-Korst component analysis[1,2] have seen extensive attention and development, and Navier-Stokes finite-difference codes have been applied to such flowfields,[3-5] an accurate and general predictive capability for base flows with large separated regions does not exist.[6]

Knowledge of the physics of these flowfields, gained through simple model experiments, has guided the development of Chapman-Korst component analyses but these past experimental efforts have provided little turbulent field or recirculating flow information. The purpose of this study was to gain a detailed knowledge of the fundamental nature of such separated compressible flows. Specifically, the turbulent mixing layers, the adjacent recirculating flow, and flowfield interactions are discussed. A related study of shear layer reattachment by Samimy et al.[7] considers other important aspects of these flows not presented herein.

Experimental Program

The flowfield configurations and experimental apparatus are discussed in the following sections. Important aspects of the laser Doppler velocimeter (LDV) instrumentation and considerations for the current flowfields are presented. The experimental results are then compared with existing data and incompressible flow results where possible.

Experimental Configurations

Three backward-facing step flowfields were investigated and the flowfield configuration of primary interest in this study is shown in Fig. 1. Constant pressure separation at the backward-facing step in Fig. 1 was achieved by adjusting the angle of the inclined ramp onto which the free shear layer reattached downstream of the step. For the second configuration investigated, the wind tunnel floor downstream of the step and the ramp were removed and replaced with a flat porous plate assembly through which low-momentum flow could be bled. The flowrate of the porous plate mass bleed through the wind tunnel floor downstream of the step was matched to the free shear layer entrainment rate to achieve constant pressure separation of the shear layer at the step. These two configurations allowed study of the developing mixing layer after separation without the complications of an expansion or compression at the separation point. The purpose of the porous plate mass bleed was to remove the recirculating flow and its possible effects on the adjacent shear layer by simulating a quiescent semi-infinite fluid boundary condition in a small-scale wind tunnel. The reattachment and redevelopment of the mixing layer was a primary concern of Samimy et al.[8] in studying a simple backward-facing step flowfield, but mixing layer and recirculating flow data also were obtained. This is the third configuration discussed below.

A ramp configuration geometry at Mach 2.92 was used previously in studies[9,10] of shear layer reattachment and redevelopment using pressure probes and hot-wire anemometry. Samimy et al.[7] have also studied the reattachment and redevelopment process for a ramp configuration at Mach 2.46 using laser Doppler velocimetry. Ikawa and Kubota[11] examined a similar porous plate flowfield in a study of the compressible mixing layer at Mach 2.46 using hot-wire anemometry and pressure probes.

The ramp and porous plate experiments were conducted in a 101.6-mm span blow-down wind tunnel and the simple backstep experiments were conducted in a 50.8-mm span wind tunnel. Step heights were 25.4 mm for the ramp and simple backstep and 44.45 mm for the porous plate. The leading apex of the ramp was approximately 101 mm, or 3.98 step heights downstream of the base of the step. The porous plate had an

Presented as Paper 85-0177 at the AIAA 23rd Aerospace Sciences Meeting, Reno, NV, Jan. 14-17, 1985; received July 17, 1985; revision received March 18, 1986.

*Research Associate, Applied Research Laboratory. Member AIAA.
†Assistant Professor, Department of Mechanical Engineering. Member AIAA.
‡Professor and Associate Head, Department of Mechanical and Industrial Engineering. Associate Fellow AIAA.

open area 240 mm in length by 101.6 mm in span and consisted of a baffled subplenum followed by a series of six drilled 1.59-mm-thick plates 0.51 mm apart and positioned below two stacked sintered steel plates. These plates, with a combined thickness of 6.35 mm, were the wind tunnel floor.

The ramp angle and the porous plate mass bleed were adjusted for constant pressure separation by viewing the flow with a Schlieren system. Side wall static pressure measurements were also made to determine that the constant pressure separation had been achieved. A 19.4 deg ramp angle was used.

Experimental Flow Conditions

The approach flow to the ramp and porous plate test sections was at Mach 2.43 with a stagnation temperature of 298 ± 4 K and a stagnation pressure of 551.6 kPa. This produced a freestream velocity of approximately 570 m/s with a unit Reynolds number of 5.57×10^7/m. For the simple backward-facing step flowfield, a Mach 2.07 approach flow expanded to Mach 2.74 at the step. The freestream velocity adjacent to free shear layer after the expansion and separation at the step was approximately 594 m/s with a unit Reynolds number of 6.69×10^7/m.

The mixing layer reattached onto the ramp 4.5 mm below the level of the step (see Fig. 2). Although the reattachment line was straight and horizontal, the flow was not two-dimensional but developed spanwise cells. Measurements made 19.05 mm off the wind tunnel centerplane showed that the variation of the mean streamwise velocity with center plane values was 2.2–2.7% of the freestream velocity in the region of maximum velocity gradient in the mixing layer and less elsewhere. The standard deviations of the corresponding streamwise component velocity fluctuations were 0.2–0.5% of the freestream velocity greater that the centerplane values. These differences are comparable to those that would result from a shift of the mixing layer of approximately 0.13 mm transverse to the freestream direction. This is twice the estimated limit of the precision with which the LDV measurement volume could be repositioned in the transverse direction after rezeroing, as was done for these off-center measurements. The 50.8-mm span wind tunnel results were similar.[7,8]

The LDV System

A two-channel coincident LDV system with forward scatter light collection at 10 deg off axis was used. The measurement volume diameter was approximately 0.13 mm for the ramp and porous plate experiments. The effective length of the measurement volume was approximately 0.9 mm. A longer focal length lens producing a 0.30-mm-diam measurement volume and a correspondingly larger fringe spacing was used in the simple backstep experiments.

One laser beam in each LDV channel was frequency shifted at 40 MHz to allow determination of the velocity direction and to reduce fringe bias. The fringes were oriented at $\pm$ 45 deg to the freestream direction to minimize any fringe bias.[12] Approach flow boundary-layer data near the wall were taken with only the streamwise velocity component measured due to beam blockage.

The small scale of the experiments and the large velocity gradients across shear layers could have led to errors due to poor spatial resolution. Estimates of the effects of the spatial resolution, after Karpuk and Tiederman,[13] were made. The worst-case error occurred initially after separation. For the ramp, this error was 1.1% in the mean streamwise velocity and 2.8% in the standard deviation of the streamwise component velocity fluctuations. The resultant increase in the streamwise component turbulent intensity was 0.41%. These errors decreased substantially downstream of the separation point as the gradients diminished.

All flows were artificially seeded with atomizers using a 50-cP silicone oil. The wind tunnel plenum and the porous plate mass bleed were seeded but the recirculating flows of the ramp and simple backstep were not directly seeded. The plenum seed was passed through a 1-μm oil mist filter prior to injection. The ratio of the LDV data rate to the local mass flowrate was nearly the same in the ramp recirculating and freestream flows. This indicates that particles were transported across the streamline discriminating between the flow in the mixing layer that escapes from the base at reattachment and that which is returned to the base sufficiently well such that the particle concentration did not change significantly across the mixing layer.

An estimate was made of the mean diameter of the seed particles by examining the velocity relaxation of the particles downstream of an oblique shock wave. Comparison of the results with calculations using the empirical drag coefficient correlation of Walsh[14] indicated a 1-μm mean aerodynamic diameter was seen by the LDV.[15] The expected frequency response of such particles is 25–30 kHz.[15-17] From the moving frame of the particles, this should have been sufficient for response to the energy-containing eddies and for accurate estimation of the turbulent stresses.

The number of samples taken at a data location was determined by the data rate and the local turbulence intensity. Only 1024 samples were taken in the freestream flow due to the low turbulence levels there but 4096 samples were taken in the mixing layer. Either 1024 or 2048 samples were taken in the low-

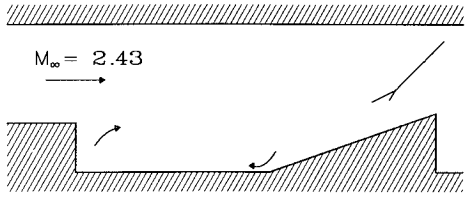

Fig. 1 Ramp configuration backward-facing step flowfield.

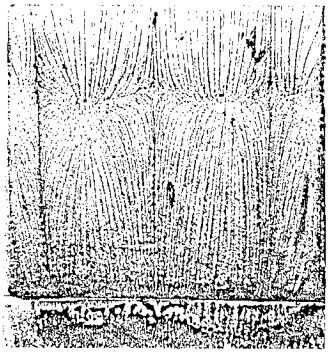

Fig. 2 Surface oil flow visualization of the free shear layer reattachment onto the ramp. The freestream flow moves from the bottom to the top.

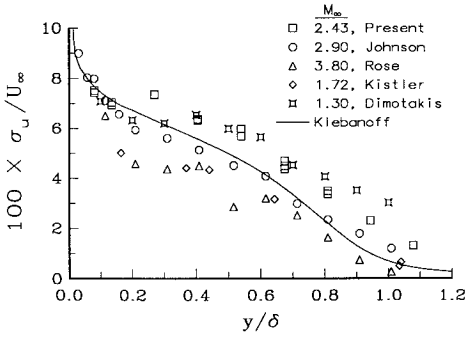

Fig. 3 Streamwise component boundary-layer turbulence intensity profiles taken by various researchers with hot-wire anemometers and LDV and the present data.

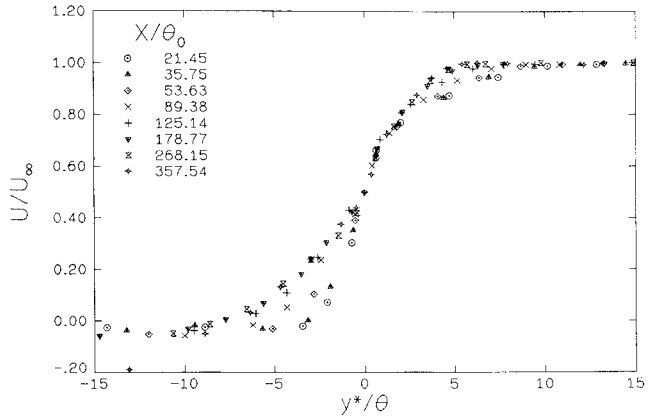

Fig. 4 Mean U component velocity profiles in similarity coordinates for the ramp mixing layer.

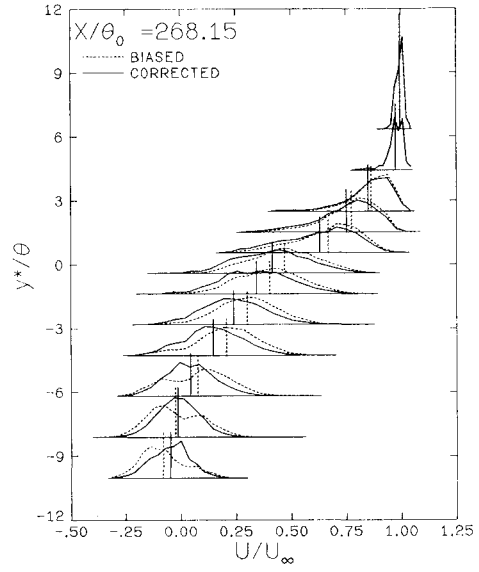

Fig. 5 U component velocity-biased and two-dimensional velocity bias-corrected PDF's across the mixing layer in the ramp flowfield.

velocity, low-data rate recirculating flow. Mixing layer and recirculating flow data were sampled in two sequential wind tunnel runs per location due to the 90 s maximum run times in the larger blow-down wind tunnel.

The Approach Boundary Layer

The 99% and momentum thicknesses of the approach boundary layer for the ramp and porous plate test sections at the step, δ_0 and θ_0, were 3.71 mm and 0.28 mm, respectively. This agrees with pressure probe results, to within 2.5%, obtained by Hampton and White.[18] The momentum-to-boundary-layer-thickness ratio was 0.075, which is approximately 12% larger than the result of the formulation of Maise and McDonald.[19]

A one-sixth power-law profile fit the mean streamwise component boundary-layer velocity profile well. A modified law of the wall (see Maise and McDonald[19]) with the Van Driest compressibility transformation was also fit to the velocity profile. This allowed estimation of the skin friction coefficient, $C_f = 0.00142$, for the ramp and porous plate boundary layers. This value is comparable with the results of others.[7,9]

The boundary-layer streamwise-component turbulent intensity profile of the present study generally agrees with other data, as shown in Fig. 3. The LDV data of Johnson[20] and Dimotakis et al.,[21] and the hot-wire data of Kistler[22] and Rose,[23] are shown with a curve for Klebanoff's incompressible result.[24] The data of the current study follow Klebanoff's curve but is above it through most of the boundary layer. LDV boundary-layer data by Yanta and Lee[25] at Mach 3 and by Johnson and Rose[26] at Mach 2.9, not shown in Fig. 3, follow along but above this curve. Although the hot-wire data of Kistler[22] and Rose[23] fall below the other data in the lower half of the boundary layer, the later hot-wire results in Ref. 26 do not. The high freestream levels of turbulence intensity in Fig. 3 were the result of the clock count resolution of the Doppler signal processors. In the current study, the freestream turbulence is estimated as less than 0.5%.

The boundary-layer profiles of the Reynolds shear stress fluctuation term, $\langle u'v' \rangle$, are similar to those of others.[7,20,25] These boundary-layer shear stress results follow Sanborn's[27] "best estimate" for equilibrium boundary layers closely (see Samimy et al.[7]).

The Mean Flow

The mean streamwise velocity profile data for the ramp configuration indicated that the mixing layer had spread across the approach boundary-layer remnant by $X/\theta_0 = 179$. For $y<0$ and $X/\theta_0 > 179$, the ramp velocity profiles were noticeably fuller than the porous plate profiles, thus indicating greater entrainment into the mixing layer. The mixing layer momentum thickness was estimated at each X station by assuming constant pressure isoenergetic flow in the integration and by using a curve fit to the mean velocity data. For a mixing layer with a semi-infinite quiescent fluid boundary condition at negative infinity

$$\frac{d\theta}{dX} = \frac{d}{dX}\int_{-\infty}^{y_j} \frac{\rho U}{\rho_\infty U_\infty} dy$$

where y_j is the location of the dividing streamline. The mixing layer entrainment rate can be estimated, in the presence of a reverse flow, by changing the lower limit of integration to include only entrained flow. In this case the lower limit was the location where the mean streamwise velocity was $\bar{U}=0$. The entrainment rate, $d\theta/dX$, was 0.0088 for the ramp and 0.0072 for the porous plate. The Mach 2.46 porous plate result of Ikawa and Kubota[11] was $d\theta/dX = 0.0073$, or 23% less than the current ramp configuration result. The incompressible result of Liepmann and Laufer[28] is $d\theta/dX = 0.035$, which is approximately a factor of 5 greater than these porous plate entrainment rates.

The mixing layer width b, defined as the distance between the $\bar{U}/U_\infty = 0.9$ to $\bar{U}/U_\infty = 0.1$ locations was also determined at each X station. The mixing layer growth rate, db/dX, was 0.078 for the ramp mixing layer. This is 22% greater than the porous plate value of Ikawa and Kubota,[11] which is $db/dX = 0.064$. The current porous plate result was $db/dX = 0.064$. Samimy et al.[7] observed a ramp flowfield growth rate, $db/dX = 0.093$, which is 19% larger than the current ramp result. The results discussed below indicate that this difference in the two-ramp flowfield growth rates may in part be the result of the relative position of the ramp, which was 1.23 step heights closer to the backstep in the geometry studied by Samimy et al.[7]

The y coordinate has been scaled with the local shear layer momentum thickness, θ, in Fig. 4 and y^* is the distance from the $\bar{U}/U_\infty = 0.5$ location. Mean profile similarity is indicated by the collapse of the velocity profiles at the two most downstream X stations, which was also the case for the porous plate data. In the current study, mean flow similarity was observed for $X/\theta_0 > 250$ or $X/\delta_0 > 18.8$. Ikawa and Kubota[11] observed similarity for $X/\theta_0 > 275$ and Settles et al.[9] and Hayakawa et al.[10] observed similarity for $X/\delta_0 > 18$ and 17, respectively, at Mach 2.92 in a ramp flowfield. Samimy et al.[7] observed for $X/\delta_0 > 16$.

Sidewall static pressure measurements were made for all three flow configurations. The porous plate static pressures were constant with X for a distance greater than $X/\theta_0 = 600$

from the step. The ramp mixing layer static pressures were constant with X for the first two-step heights downstream of separation, through $X/\theta_0 = 90$. These mixing layer static pressures then decreased approximately 4% to a minimum at 3.5–4.0 step heights after separation; the leading edge of the ramp was at 3.98 step heights. Pressures increased downstream of this minimum but LDV data were not taken downstream of 3.94 step heights. A larger static pressure drop, 6%, was observed with the simple backward-facing step flowfield prior to the pressure rise to reattachment. The maximum reverse flow velocity was also larger in the simple backward-facing step recirculating flow—26% of the adjacent freestream velocity compared to 19% for the ramp.

The Turbulent Field

A qualitative knowledge of the turbulent field was obtained by observation of the velocity probability distribution functions (PDF). Figure 5 shows the PDF's for the U velocity component across the mixing layer at $X/\theta_0 = 268$. The horizontal lines locate the ordinate of the data and the short vertical lines mark the mean velocity. The bias referred to in Fig. 5 is the statistical sampling or velocity bias inherent to individual realization LDV. A sampling bias toward higher velocities results because the probability of obtaining a sample is dependent on the velocity magnitude, among other factors.[29] The biased distributions in Fig. 5 were obtained by adding a weighting factor of one to the histogram bin accumulator if an individual velocity realization fell within the range of the bin. All bins were of equal size. The normalized distribution was obtained by dividing the bin accumulator sums by the total sum of the weights. This is the total number of realizations in this case. The velocity-biased corrected distributions were obtained by adding a two-dimensional velocity inverse weight to the bin accumulator, w_i, where $w_i = (U_i^2 + V_i^2)^{-1/2}$ for the ith realization. Normalization was achieved by division by the total sum of these weights. The effects of any weighting function correction, such as transit time or time between data point weights on the PDF, can be visualized by this approach.

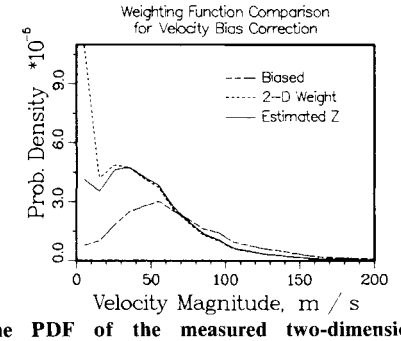

Fig. 6 The PDF of the measured two-dimensional velocity magnitude with no bias correction, with the two-dimensional velocity bias correction, and with the two-dimensional correction with the estimated Z term included, $y^*/\theta_0 = -6.56$, $X/\theta_0 = 268.15$.

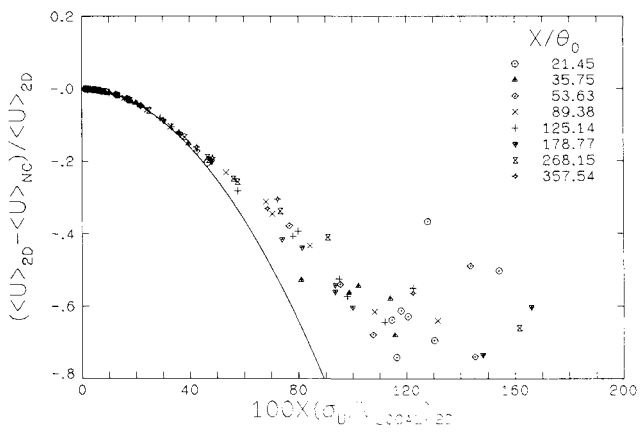

Fig. 7 Velocity bias of the ensemble averaged streamwise velocity component, $\langle U \rangle$, vs the local U component turbulence intensity with the statistical prediction of the bias by Erdmann and Tropea.[33,34]

Velocity Bias in Turbulent Flows

If velocity bias occurs in a turbulent flow as hypothesized, a distinct decrease in the probability of obtaining a sample should be observed when the total velocity magnitude is small. The mixing-layer flow of the present study is dominated by the U or streamwise velocity component such that a small magnitude U velocity correlates well with small magnitude total velocity realization. Because of this, appreciable decreases in the U component PDF's were observed at $U = 0$ in all cases where the probability at $U = 0$ was large enough to discern such details (see Fig. 5). The V component PDF's exhibit no such decrease at $V = 0$ because the transverse velocity magnitude correlates poorly with the total velocity magnitude. However, the bias is still present.

The above results indicate that velocity bias can substantially affect the velocity PDF's in these highly turbulent flows, therefore the two-dimensional velocity inverse bias correction has been used to reduce all of the data presented in this paper. This two-dimensional weighting function correction produced reasonable results but does appear to have overweighted near $U = 0$ in some cases (see Fig. 5). Recent work has found that the addition of a simple estimate of the average unmeasured Z component contribution to the velocity magnitude based on the turbulence intensities in the measured U and V components reduces the tendency of the bias correction to overweight realizations with small U and V velocities.[12] This approach has been used previously by Nakayama[30] and is discussed by Johnson et al.[31] However, the effect of this Z term on the mean velocity was less than 2% of the simple two-dimensional velocity-inverse-corrected value, which indicates overweighting was not a significant problem. Figure 6 shows the effect this estimated Z term has on the probability distribution of the measured two-dimensional velocity magnitude for the data at $y^*/\theta = -6.56$ in Fig. 5. Also, Fig. 6 indicates no noticeable compensation for velocity bias due to improved signal quality at low-velocity magnitudes.[32] Such a compensation may be effective over only a small fraction of the current velocity range and is likely to have a signal-to-noise ratio dependence.

The velocity bias effect on the mean U component as a function of the streamwise turbulence intensity, based on the magnitude of the local mean velocity, is shown in Fig. 7. The NC subscript refers to the result with no correction and 2D refers to the bias corrected result. The curve in Fig. 7 is the predicted form of the bias obtained by the statistical analysis of Erdmann and Tropea.[33,34] The current LDV sampling process was at low burst and data density with a free-running processor. The bias in the mean velocity is predicted to equal the turbulence intensity squared. The analysis is consistent with the two-dimensional corrected results, and the low-speed mixing-layer data of Johnson et al.[31] show a similar trend. Turbulence intensities based on the local mean velocity for $y^*/\theta < 0.0$ were 30% or larger.

Examination of the effects of the bias on flowfield statistics has shown that the biased standard deviations of the velocity distributions differ by less than ±10% with the bias-corrected values in most of the flowfield, but this difference may be as large as −20%.[12] The differences between the biased and corrected Reynolds shear stress term, $\langle u'v' \rangle$, were twice as large as for the normal stresses. This indicates that the largest deviations from the mean contribute most significantly to the shear stress.

Turbulent Field Characteristics

The velocity PDF's in Fig. 5 skew out at the freestream edge of the mixing layer, developing a long flat tail on the low-speed side of the mean of the distribution. The dynamic range

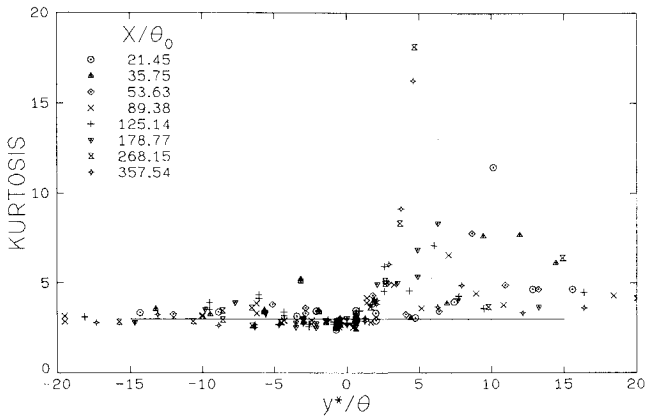

Fig. 8 Profiles of the U velocity component kurtosis factor for the ramp configuration flowfield.

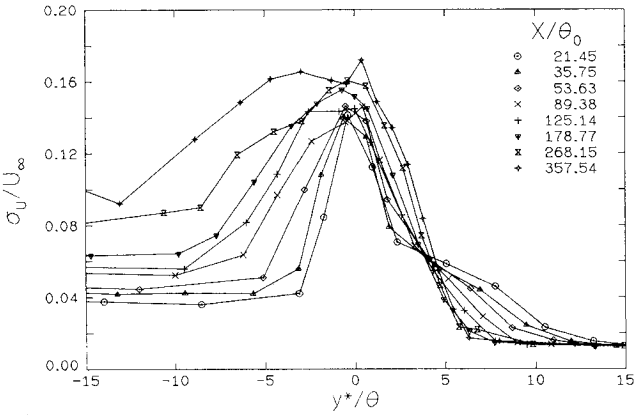

Fig. 9 Streamwise component turbulence intensity profiles for the ramp flowfield.

of velocity fluctuations increased to a maximum at $y^*/\theta = 0.0$ and the distribution filled out, taking on a Gaussian form. The dynamic range decreased as the low-speed edge or recirculating flow side of the mixing layer was approached, and skewing of the PDF in an opposite sense to that at the freestream side occurred. The observed behavior is similar to what Davies[35] observed in a low-speed round jet traversing from the potential core across the jet into a quiescent ambient fluid.

These features of the PDF's are also seen in the higher-order central moments of the distributions. Figure 8 shows the normalized fourth-order central moment or kurtosis factor results for the U component in the ramp flowfield. The porous plate results are similar. A higher-order moment is most affected by and weights most heavily the larger excursions from the mean of the distribution. The large kurtosis factors at the high-speed side of the mixing layer correspond to the long, flat tails in the PDF's of Fig. 5. A few kurtosis values on this side of the mixing layer were too large to be shown in Fig. 8 as it is scaled. The kurtosis values in the core of the mixing layer were actually slightly less than the indicated Gaussian value of 3. A subtle kurtosis peak occurred at the low-speed edge of the mixing layer. These kurtosis factor results are similar to incompressible mixing-layer results with one exception. The incompressible mixing layer exhibits a peak value at the low-speed edge that is as large or larger than on the high-speed side.[36,37] This indicates that comparatively fewer large-scale fluctuations and entraining motions occur on the low-speed side of the compressible mixing layer. The observed factor of 5 decrease of the entrainment rates, relative to incompressible flow, support that this should be the case. However, Hayakawa et al.[10] observed mass flowrate kurtosis profiles in a Mach 2.92 mixing layer similar to the incompressible result. The skewness factor or third-order normalized central moment results also differed with the incompressible mixing-layer behavior in that the peak values on the low-speed side were typically less than half of those on the high-speed side, opposite to the incompressible case.[36,37]

Turbulence intensity profiles for the ramp configuration flowfield are shown in Fig. 9 for the U velocity component. These profiles did not collapse together as the mean profiles did in Fig. 4. However, scaling with the local maximum intensity did collapse the data for $y^*/\theta > 0.0$. The turbulence intensities on the low-speed side of the mixing layer were noticeably higher in the ramp flow than in the porous plate flow for $X/\theta_0 > 178$ where the ramp recirculating flow velocities were largest. The maximum U component intensities occurred at $y^*/\theta = 0$, which is the same as observed in the incompressible mixing layer.[36,37] The V component intensity profiles peaked on the low-speed side of the mixing layer. This is opposite to the incompressible mixing layer for which the shift is toward the high-speed side.

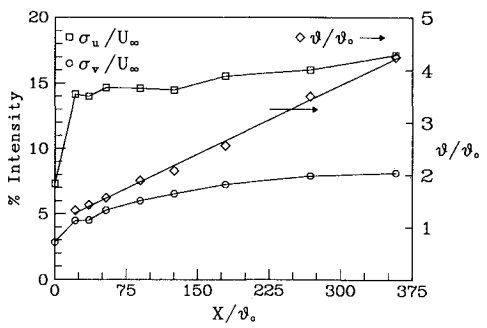

Fig. 10 Local maximum turbulence intensities and momentum thicknesses for the ramp flowfield mixing layer. The linear least-squares fit to the momentum thickness data, used to estimate the entrainment rate, is shown.

The local maximum turbulence intensities vs X/θ_0 for the ramp are shown in Fig. 10. Also, the ramp mixing layer momentum thicknesses with a linear least-squares fit are included in Fig. 10. The initial boundary layer intensity values shown are less than the true maximum values because beam blockage limited the proximity to which the wall could be approached (see Fig. 3). The U component intensity remained nearly constant initially but increased from 14.6% after separation to 17.2% at the base of the ramp. An increase in mass flowrate intensities with increasing X was observed previously.[9,10] Porous plate maximum intensities remained near the 15% level, indicating that the interaction between the mixing layer and the recirculating flow leads to the downstream intensity increase. However, the V component maximum turbulence intensity asymptotically approached 8.2% and does not appear to have been affected by the recirculating flow since the porous plate results were nearly the same. Such an increase in the U component intensity with no increase in the V component values would be observed if the mixing layer were subject to small transverse oscillations as the ramp and the reattachment were approached. The velocity-biased corrected U component PDF at $X/\theta_0 = 357.54$, $y^*/\theta = -6.36$ (see Fig. 4) was slightly bimodal about $U = 0$. This indicates that this stagnant measurement location was alternately in the entrained mixing-layer flow or the reversed recirculating flow and that some larger scale motion and unsteadiness was present at the base of the ramp.

The turbulent intensities in incompressible mixing layers are larger than observed in the present compressible flow. Champagne et al.[6] observed 17.1% and 11.7% values for the U and V component maximum turbulence intensities, respectively, in an incompressible mixing layer. The current V component maximum intensities were one-third to one-half of the U com-

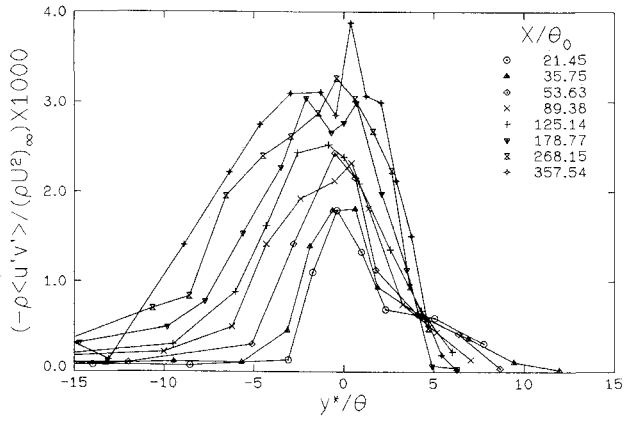

Fig. 11 Reynolds shear stress profiles for the ramp flowfield.

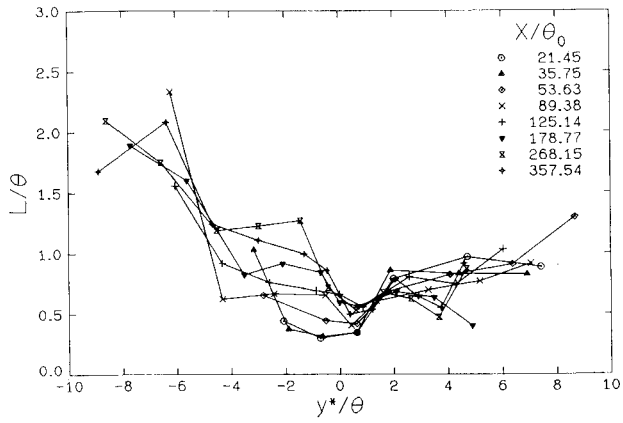

Fig. 12 Mixing length profiles for the ramp flowfield, $L = |\langle u'v' \rangle|^{1/2}/(d\bar{U}/dy)$.

ponent values but this ratio is approximately two-thirds for the incompressible mixing layer. An order-of-magnitude analysis by Brown and Roshko[38] indicates that the transverse component intensity should decrease as Mach number increases in supersonic flow.

The available hot-wire turbulence data differ with the current results. Wagner[39] did not make measurements in the transonic core of a Mach 5.0 mixing layer. This was because of the reported difficulties with the hot-wire calibration at transonic Mach numbers.[39,40] An extrapolated estimate of the maximum streamwise turbulent intensity was 9%. Ikawa and Kubota[11] observed a maximum streamwise component turbulent intensity of 5-6%. This is much less than the current result of approximately 15% after separation and significantly less than in the approach boundary layer. Ikawa and Kubota also observed the peak streamwise intensity occurring decidedly on the high-speed side of the mixing layer, where the mean density gradient is large, and away from the maximum gradient of the U velocity component. The hot-wire results of Hayakawa et al.[10] were presented in terms of mass flowrate fluctuation level and were similar to the mass flowrate results of Ikawa and Kubota.[11] The velocity fluctuation intensity profiles of Ikawa and Kubota, reduced from hot-wire mass flowrate fluctuation data, resemble the mass flowrate profiles in form. However, the boundary-layer mass flowrate fluctuation intensity profiles of Hayakawa et al.[41] do not resemble the velocity fluctuation profiles of Fig. 3, and no sharp peak is observed in the mixing-layer mass flowrate intensity near $y^* = 0$ where the maximum velocity gradients occur.[9,10]

The current maximum intensity estimates are subject to error sources that would falsely increase the turbulence level. The combined effect of the spatial resolution and processor clock count resolution is estimated to increase these maximum intensities by as much as 1.0% near the step and 0.65% at downstream locations. Electronic noise also increases the turbulence intensity falsely but no procedure for accurately estimating the noise effect was carried out. Particle dynamics could also have a potential effect on the turbulence statistics.

Reynolds shear stress results for the ramp flowfield are given in Fig. 11. The density was estimated by assuming constant pressure isoenergetic flow across the mixing layer. The local maximum Reynolds stress occurs on the low-velocity side of the mixing layer. The shift to the low-velocity side is more pronounced for the $\langle u'v' \rangle$ term alone; approximately 85% of the factor of 2.2 density decrease across the mixing layer occurred above the $y^*/\theta = 0$ location. This shift is opposite to that observed in an incompressible mixing layer which is toward the high-speed side.[36,37] The maximum shear stresses Ikawa and Kubota[11] determined from their mean profile data, $\tau_{max}/(\rho_\infty U_\infty^2) = 0.0028$, are comparable to the values measured directly with the LDV in the current study. The incompressible mixing-layer result of Wygnanski and Fiedler[37] is approximately triple the current result, $\tau_{max}/(\rho_\infty U_\infty^2) = 0.0092$. The decrease of the density from the high- to the low-speed side of the mixing layer accounts for half of the reduction of the compressible flow shear stress relative to incompressible results. The reduced V component turbulence intensity and, therefore, transverse transport capability in the compressible mixing layer also reduces the shear stress. The correlation coefficient, $R_{uv} = \langle u'v' \rangle/\sigma_u\sigma_v$, was typically -0.5 to -0.58 in the ramp and porous plate mixing layers. This is similar to the incompressible results of Patel[42] (-0.54), and of Liepmann and Laufer[28] (-0.57).

Relative to the local maximum value, the shear stresses in the recirculating flow were much smaller than the normal stresses were in Fig. 9. These large normal stresses and relatively small shear stresses suggest that a pulsation or unsteadiness is a feature of the recirculating flow.

Samimy et al.[7] have observed that the reattachment region of these separated flowfields exhibit large increases in the turbulent triple product terms, indicating the development of large-scale structures and motions. Settles et al.[9] have also observed the development of large eddies at reattachment. The reattachment region appears to be a potential source for the unsteadiness observed in the present flow.

The normal stress results in the simple backward-facing step flowfield differed from the ramp flow. The U component direction is defined as parallel to the shear layer after the expansion at the separation corner. The U component turbulence intensities in the free shear layer reached 21% prior to the beginning of the pressure rise preceding reattachment. The V component intensities, which were slightly less than the ramp and porous plate values, reached 7.3% before the beginning of the pressure rise. The normal stresses in the recirculating flow were slightly higher than those observed in the ramp flowfield. Reynolds shear stresses reached values nearly double those in the ramp mixing layer and the maximum local correlation coefficient values were -0.6 to -0.8. The shear layer reattached only 2.76 step heights downstream of the step. The unsteady reattachment process appears to contaminate the entire recirculating flow and the adjoining shear layer in this simple backward-facing step flowfield.

An estimate of the turbulent kinetic energy, k, was made by assuming

$$k = \tfrac{1}{2}[\overline{u'^2} + \overline{v'^2} + \tfrac{1}{2}(\overline{u'^2} + \overline{v'^2})] = \tfrac{3}{4}(\overline{v'^2} + \overline{u'^2})$$

The ratio of the Reynolds shear term, $-\langle u'v' \rangle$, to the estimated TKE was examined. The often-cited value for this correlation for a variety of shear flows is 0.3,[43] and this was a typical value on the subsonic side of the mixing layer. However, a decrease to lower values was observed in the transonic and supersonic regions of the mixing layer where typical values were 0.23-0.25.

The apparent kinematic viscosity, $|\langle u'v'\rangle/(d\bar{U}/dy)|$, increased dramatically on the low-speed side of the ramp flow mixing layer for $X/\theta_0 > 178$. This increase in the shear stresses relative to the local mean flow gradient is indicative of an increase in larger scale fluctuations.

The turbulent mixing length, $|\langle u'v'\rangle|^{1/2}/(d\bar{U}/dy)$, is shown in Fig. 12 for the ramp flowfield nondimensionalized with the mixing layer momentum thickness. Mixing-layer momentum thickness growth was nearly linear with the distance from the separation point (see Fig. 10), therefore the mixing length growth with X was nearly linear. The porous plate results were similar but values of the mixing length were smaller at the low-speed edge of the mixing layer by 25–50%. The ratio of the shear layer width, b, to the mixing length is $1/32 < L/b < 1/4$ across the mixing layer.

Conclusions

An experimental study of compressible separated flows using a two-channel LDV system and three backward-facing step flowfield configurations was conducted. Mixing-layer growth and entrainment rates were much less than those observed in incompressible flow, as expected. The profiles of turbulence intensity, shear stress, and the kurtosis and skewness factors indicate that the compressible mixing layer is structured differently from the incompressible counterpart. Transverse component turbulent intensities and Reynolds shear stresses in compressible mixing layers are substantially less and the turbulence field substantially more anisotropic than in the incompressible counterpart. In the presence of a recirculating flow, increased mixing-layer growth and entrainment rates were observed. This appears to be the result of the unsteady character of the free shear layer reattachment process and how these disturbances propagate into the recirculating flow. LDV velocity bias was observed and two-dimensional velocity inverse correction worked reasonably well. This correction was improved by the inclusion of an estimated Z component term to the corrective weight.

Acknowledgments

This research was supported by the U.S. Army Research Office under Contracts DAAG 29-79-C-0184 and DAAG 29-83-K-0043. Dr. Robert E. Singleton served as contract monitor.

References

[1]Chapman, D. R., "An Analysis of Base Pressure at Supersonic Velocities and Comparison with Experiment," NACA TN 2137, 1950.

[2]Korst, H. H., "A Theory for Base Pressure in Transonic and Supersonic Flow," *Journal of Applied Mechanics,* Vol. 23, 1956, pp. 593–600.

[3]Hasen, G. A., "Navier-Stokes Solutions for an Axisymmetric Nozzle in a Supersonic External Stream," AFWAL-TR-3161, March 1982.

[4]Horstmann, C. C., Settles, G. S., Bogdonoff, S. M., and Williams, D. R., "A Reattaching Free Shear Layer in Compressible Turbulent Flow—A Comparison of Numerical and Experimental Results," *AIAA Journal,* Vol. 20, Jan. 1984, pp. 79–85.

[5]Weinberg, B. C., McDonald, H., and Shamroth, S. J., "Navier-Stokes Computations of Aft End Flow Fields," U.S. Army Research Office Final Report Contract DAAG 29-79-C-0003, Scientific Research Associates, Inc., Glastonbury, CT, May 1982.

[6]Petrie, H. L. and Walker, B. J., "Comparison of Experiment and Computation for a Missile Base Region Flow with a Centered Propulsive Jet," AIAA Paper 85-1618, July 1985.

[7]Samimy, M., Petrie, H. L., and Addy, A. L., "A Study of Compressible Turbulent Reattaching Free Shear Layers," *AIAA Journal,* Vol. 24, Feb. 1986, pp. 261–267.

[8]Samimy, M., Petrie, H. L., and Addy, A. L., "Reattachment and Redevelopment of Turbulent Free Shear Layers," *International Symposium on Laser Anemometry,* FED-Vol. 33, 1985, pp. 159–166; also presented at the ASME Winter Annual Meeting, Nov. 1985.

[9]Settles, G. S., Baca, B. K., Williams, D. R., and Bogdonoff, S. M., "A Study of Reattachment of a Free Shear Layer in Compressible Turbulent Flow," *AIAA Journal,* Vol. 20, Jan. 1984, pp. 60–67.

[10]Hayakawa, K., Smits, A. J., and Bogdonoff, S. M., "Turbulence Measurements in a Compressible Reattaching Shear Layer," *AIAA Journal,* Vol. 22, July 1984, pp. 889–895.

[11]Ikawa, H. and Kubota, T., "Investigation of Supersonic Turbulent Mixing Layer with Zero Pressure Gradient," *AIAA Journal,* Vol. 13, May 1975, pp. 566–572.

[12]Petrie, H. L., Samimy, M., and Addy, A. L., "An Evaluation of LDV Velocity and Fringe Bias Effects in Separated High Speed Turbulent Flow," *ICIASF Record '85,* edited by F. K. Owen, IEEE, New York, Aug. 1985, pp. 297–308.

[13]Karpuk, M. E. and Tiederman, W. G. Jr., "Effect of Finite Size Probe Upon Laser Doppler Anemometer Measurements," *AIAA Journal,* Vol. 14, Aug. 1976, pp. 1099–1105.

[14]Walsh, M. J., "Influence of Particle Drag Coefficient on Particle Motion in High-Speed Flow with Typical Laser Velocimetry Applications," NASA TN D8120, 1976.

[15]Petrie, H. L., "A Study of Compressible Turbulent Free Shear Layers Using Laser Doppler Velocimetry," Ph.D. Dissertation, Dept. of Mechanical and Industrial Engineering, Univ. of Illinois at Urbana-Champaign, Urbana, IL, April 1984.

[16]Sommerscales, E. F. C., "The Dynamic Characteristics of Flow Tracing Particles," *Proceedings of the 2nd International Workshop on Laser Velocimetry,* Vol. 1, Purdue University, West Lafayette, IN, March 1974, pp. 216–233.

[17]Mazumder, M. K. and Kirsch, K. J., "The Flow Tracing Fidelity of Scattering Aerosol in Laser Doppler Velocimetry," *Applied Optics,* Vol. 14, No. 4, April 1975, pp. 884–901.

[18]Hampton, L. P. and White, R. A., "The Effect of Sudden Expansions and Compressions on Turbulent Boundary Layer Momentum Thickness in Supersonic Flow," University of Illinois at Urbana-Champaign, Urbana, IL, Rept. UILU-ENG-83-4004, 1983.

[19]Maise, G. and McDonald, H., "Mixing Length and Kinematic Eddy Viscosity in a Compressible Boundary Layer," *AIAA Journal,* Vol. 6, Jan. 1968, pp. 73–80.

[20]Johnson, D. A., "Turbulence Measurements in a Mach 2.9 Boundary Layer Using Laser Velocimetry," *AIAA Journal,* Vol. 12, May 1974, pp. 711–714.

[21]Dimotakis, P. E., Collins, D. J., and Lang, D. B., "Laser Doppler Velocity Measurement in Subsonic, Transonic, and Supersonic Turbulent Layers," *Laser Velocimetry and Particle Sizing,* edited by H. D. Thompson and W. H. Stevenson, Hemisphere, New York, 1979, pp. 208–219.

[22]Kistler, A. L., "Fluctuation Measurements in a Supersonic Turbulent Boundary Layer," *The Physics of Fluids,* Vol. 2, No. 3, March 1959, pp. 290–297.

[23]Rose, W. C., "Turbulence Measurements in a Compressible Boundary Layer Subject to a Shock-Wave Induced Adverse Pressure Gradient," AIAA Paper 73-167, 1973.

[24]Klebanoff, D. S., "Characteristics of Turbulence in a Boundary Layer with Zero Pressure Gradient," NACA Rept. 1247, 1955.

[25]Yanta, W. J. and Lee, R. E., "Measurements of Mach 3 Turbulence Transport Properties on a Nozzle Wall," *AIAA Journal,* Vol. 14, June 1976, pp. 725–729.

[26]Johnson, D. A. and Rose, W. C., "Laser Velocimeter and Hot-Wire Anemometer Comparison in a Supersonic Boundary Layer," *AIAA Journal,* Vol. 13, April 1975, pp. 512–515.

[27]Sanborn, V. A., "A Review of Turbulence Measurements in Compressible Flow," NASA TM X-62-337, March 1974.

[28]Liepmann, H. W. and Laufer, J., "Investigation of Free Turbulent Mixing," NACA TN 1257, 1947.

[29]McLaughlin, D. K. and Tiederman, W. G. Jr., "Biasing Correction for Individual Realization of Laser Anemometer Measurements in Turbulent Flow," *The Physics of Fluids,* Vol. 16, No. 12, Dec. 1973, pp. 2082–2088.

[30]Nakayama, A., "Measurements of a Separating Boundary Layer and Wake of an Airfoil Using Laser Doppler Velocimetry," AIAA Paper 85-0181, Jan. 1985.

[31]Johnson, D. A., Modarress, D., and Owen, F. K., "An Experimental Verification of Laser Velocimeter Sampling Bias and Its Correction," *Engineering Applications of Laser Velocimetry,* ASME, New York, 1982, pp. 153–162.

[32]Durao, D. F. G. and Whitelaw, J. H., "Relationship Between Velocity and Signal Quality in Laser Doppler Anemometry," *Journal of Physics, E: Scientific Instruments,* Vol. 12, No. 1, Jan. 1979, pp. 47–50.

[33]Erdmann, J. C. and Tropea, C., "Statistical Bias of the Velocity Distribution Function in Laser Anemometry," International Symposium on Applications of Laser Doppler Anemometry to Fluid Mechanics, Lisbon, Portugal, July 1982, Paper 16.2.

[34]Erdmann, J. C. and Tropea, C., "Turbulence Induced Statistical Bias in Laser Anemometry," *Proceedings of the Seventh Symposium on Turbulence,* University of Missouri-Rolla, Sept. 1981, pp. 129-138.

[35]Davies, P.O.A.L., "Turbulence Structure in Free Shear Layers," *AIAA Journal,* Vol. 4, Nov. 1966, pp. 1971-1978.

[36]Champagne, F. H., Pao, Y. H., and Wygnanski, I. J., "On the Two-Dimensional Mixing Region," *Journal of Fluid Mechanics,* Vol. 74, Pt. 2, 1976, pp. 209-250.

[37]Wygnanski, I. J. and Fiedler, H. E., "The Two-Dimensional Mixing Region," *Journal of Fluid Mechanics,* Vol. 41, 1970, pp. 327-361.

[38]Brown, G. L. and Roshko, A., "On Density Effects and Large Structure in Turbulent Mixing Layers," *Journal of Fluid Mechanics,* Vol. 64, Pt. 4, 1974, pp. 775-816.

[39]Wagner, R. D., "Mean Flow and Turbulence Measurements in a Mach 5 Free Shear Layer," NASA TN D7366, 1973.

[40]Smits, A. J., Hayakawa, K., and Muck, K. C., "Constant Temperature Hot-Wire Anemometer Practice in Supersonic Flows—Part 1-The Normal Wire," AIAA Paper 83-0050, Jan. 1983.

[41]Hayakawa, K., Smits, A. J., and Bogdonoff, S. M., "Hot-Wire Investigation of an Unseparated Shock-Wave/Turbulent Boundary Layer Interaction," *AIAA Journal,* Vol. 22, May 1984, pp. 579-585.

[42]Patel, R. P., "An Experimental Study of a Plane Mixing Layer," *AIAA Journal,* Vol. 11, Jan. 1973, pp. 67-71.

[43]Harsha, P. T. and Lee, S. C., "Correlation Between Turbulent Shear Stress and Turbulent Kinetic Energy," *AIAA Journal,* Vol. 8, Aug. 1970, pp. 1508-1510.